2-D CONSTANT-OFFSET DIFFRACTION SEPARATION

E. G. Asgedom, L.-J. Gelius, and M. Tygel

email: *mtygel@gmail.com*

keywords: *Seismic Processing, Seismic Imaging, Traveltime, Common-Offset, CRS*

ABSTRACT

Diffractions contain the most valuable information about small-scale inhomogeneities and discontinuities in the subsurface. In this paper we propose a diffraction separation technique that works directly in the common-offset domain. The method is based on a modified CRS- equation tailored for diffractions. By introducing a constant-offset reference ray, large offsets can also be handled as demonstrated employing both synthetic and field data.

INTRODUCTION

Seismic diffracted waves may carry high-resolution information about key subsurface structures associated with potential hydrocarbon traps. However, the amplitudes of these waves are in general much weaker than those of the reflected waves. During the last years, different approaches have therefore been proposed to separate diffractions from reflections. Such techniques either work pre-stack or post-stack. Examples of the latter are the use of plane-wave destruction filters (Fomel, 2002; Fomel et al., 2007) and a modified version of the Common Reflection Surface (CRS) technique (Asgedom et al., 2011).

Landa et al. (1987) proposed the use of a specialized double-square-root traveltime moveout to enhance diffractions in a common-offset section. In this paper an alternative constant- offset diffraction separation technique is proposed. It is based on a modified CRS-equation tailored for diffractions and employing a constant-offset central ray. By replacing the ZO reference ray with that of constant offset, succesfull diffraction separation can also be obtained for large offsets. The potential of the method is demonstrated using controlled data as well as multi-offset GPR data.

FORMULATION

For a given fixed (central) ray, propagating from the source, $S^0(s^0)$ via a reflecting interface back to the receiver, $G^0(g^0)$, the hyperbolic 2-D traveltime formula of a reflected paraxial ray joining the neighboring source and receiver pair, $S(s)$ to $G(g)$ have the form (see, e.g. Ursin, 1982)

$$t^2(s,g) = (t_0 - p_S\Delta s + p_G\Delta g)^2 + t_0(-2M_{sg}\Delta s\Delta g + M_{ss}\Delta s^2 + M_{gg}\Delta g^2)\,, \tag{1}$$

where

$$\Delta s = s - s_0, \quad \Delta g = g - g_0. \tag{2}$$

Here, the first-order coefficients, p_S and p_G are the slowness of the central ray tangential to the respective measurement surfaces,

$$p_S = \frac{\partial t}{\partial s}(s^0, g^0) = \frac{\sin\beta_S}{v_S}, \quad p_G = \frac{\partial t}{\partial g}(s^0, g^0) = \frac{\sin\beta_G}{v_G}, \tag{3}$$

with v_S and β_S being respectively the near-surface velocity and take-off angle of the central ray at the source S^0, with analogous definitions for the quantities v_G and β_G. In the same way, the second-order

coefficients are given by (see Ursin, 1982)

$$M_{sg} = \frac{\partial^2 t}{\partial s \partial g}(s^0, g^0), \quad M_{ss} = \frac{\partial^2 t}{\partial s^2}(s^0, g^0), \quad M_{gg} = \frac{\partial^2 t}{\partial g^2}(s^0, g^0). \tag{4}$$

Following Zhang et al. (2001), introduce the following three wavefront curvatures: (i) K^g_{CS} observed at G^0 associated with a wave starting from a point source at S^0 (common-source geometry), (ii) K^g_{CMP} observed at G^0 associated with a wave consisting of the central ray and its paraxial rays in the vicinity of S^0 (CMP-geometry) and (iii) characterized by K^s_{CMP} when observed at S^0. The coefficients M_{sg}, M_{ss} and M_{gg} in Eq. (1) can now be expressed by these wavefront curvatures as follows (Zhang et al., 2001):

$$\begin{aligned} M_{sg} &= \frac{(K^G_{CMP} - K^G_{CS})\cos\beta^2_G}{v_G}, \\ M_{ss} &= -\frac{K^S_{CMP}\cos^2\beta_S}{v_S} - \frac{(K^G_{CMP} - K^G_{CS})\cos^2\beta_G}{v_G}, \\ M_{gg} &= \frac{K^G_{CS}\cos^2\beta_G}{v_G}. \end{aligned} \tag{5}$$

Diffraction separation in the midpoint-offset domain

The hyperbolic traveltime formula in Eq. (1) is tailored for reflected events. Here we will specialize to the case of diffractions. It is then more convenient to express the traveltime formula in Eq. (1) in the midpoint-offset domain (Zhang et al., 2001):

$$t^2(m,h) = [t_0 + (p_G - p_S)\,\Delta m + (p_G + p_S)\,\Delta h]^2 + t_0[2M_{mh}\Delta m\Delta h + M_{mm}\Delta m^2 + M_{hh}\Delta h^2], \tag{6}$$

where

$$\Delta m = m - m_0 = \frac{1}{2}(\Delta g + \Delta s)\,, \quad \Delta h = h - h_0 = \frac{1}{2}(\Delta g - \Delta s), \tag{7}$$

and, moreover,

$$\begin{aligned} M_{mh} &= M_{gg} - M_{ss}, \\ M_{mm} &= M_{gg} + M_{ss} - 2M_{sg}, \\ M_{hh} &= M_{gg} + M_{ss} + 2M_{sg}. \end{aligned} \tag{8}$$

We consider now the special case of a diffractor. Introduce first the wavefront curvature of a CO-experiment with respect to the receiver side (Zhang et al., 2001):

$$\frac{\cos^2\beta_G}{v_G}K^G_{CO} = M_{gg} - M_{sg} \Rightarrow K^G_{CO} = 2K^G_{CS} - K^G_{CMP}. \tag{9}$$

As discussed by (Zhang et al., 2001), in case of a diffractor, no matter if the energy comes from a CO or CMP configuration the diffracted waves at G appear to come from a point source at the 'diffraction point'. This again implies that $K^G_{CO} = K^G_{CMP}$, which substituted into Eq. (9) yields

$$K^G_{CS} = K^G_{CMP}, \tag{10}$$

and, in turn,

$$\begin{aligned} M_{mh} &= \frac{\cos^2\beta_G}{v_G}K^G_{CMP} + \frac{\cos^2\beta_S}{v_S}K^S_{CMP} \\ M_{mm} = M_{hh} &= \frac{\cos^2\beta_G}{v_G}K^G_{CMP} - \frac{\cos^2\beta_S}{v_S}K^S_{CMP}. \end{aligned} \tag{11}$$

Zero-offset central ray and constant-offset diffraction separation

In case of a ZO central ray the source S^0 will move and coincide with the receiver G^0 , and the following relations hold:

$$\beta = \beta_G = -\beta_S\,, \quad v = v_G = v_S, \quad p = -p_S = p_G, \quad K_{NIP} = K^G_{CMP} = -K^S_{CMP}\,, \tag{12}$$

which in combination with Eq. (6) gives the 'classical' CRS-equation in case of diffractions:

$$t^2_{D,CRS}(m,h) = (t_0 + 2p\Delta m)^2 + 2t_0\frac{\cos^2\beta}{v}K_{NIP}(\Delta m^2 + h^2)\ . \tag{13}$$

Since this equation represents the traveltime function of a paraxial ray, the perturbations of both midpoint and offset have to be small. Consider now a CMP-configuration (e.g., $\Delta m = 0$), which gives the alternative version of Eq. (13):

$$t^2_{D,CRS}(m_0,h) = t^2_{CMP}(h) = t_0^2 + 2t_0\frac{\cos^2\beta}{v}K_{NIP}h^2 = t_0^2 + \frac{4h^2}{v^2_{NMO}}\ , \tag{14}$$

where we have introduced the so-called NMO-velocity.

Next, we assume a constant half-offset h_0 and rewrite Eq. (13) accordingly:

$$t^2_{D,CO}(m,h_0) = (t_{CMP}(h_0) + a_{CO}\Delta m)^2 + b_{CO}\Delta m^2\ , \tag{15}$$

with the introduction of the parameters

$$a_{CO} = \frac{2\sin\beta}{v} = 2p\ , b_{CO} = \frac{4}{v^2_{NMO}}\ . \tag{16}$$

Equation (15) can now be used to enhance diffractions within a *constant-offset (CO)* section. In practice this could be implemented as a two-step procedure: (i) determine NMO-velocity from Eq. (14) and parameter a_{CO} from Eq. (15) using a coherency analysis and (ii) stack data according to Eq. (15) choosing a proper aperture. The main problem with this formulation is that it is valid only for smaller offsets. In order to handle larger offset, the ZO central ray should be replaced by a CO central ray.

Constant-offset central ray and constant-offset diffraction separation

The starting point now is based on Eq. (6) and Eq. (11). Consider first a CMP-sorting which simplifies Eq. (6) as follows:

$$\begin{aligned} t^2_D(m_0,h) &= t^2_{CMP}(\Delta h) = [t_0 + (p_S + p_G)\,\Delta h]^2 \\ &+ t_0\left(\frac{\cos^2\beta_G}{v_G}K^G_{CMP} - \frac{\cos^2\beta_S}{v_S}K^S_{CMP}\right)\Delta h^2\ , \end{aligned} \tag{17}$$

or alternatively,

$$t^2_{CMP}(\Delta h) = (t_0 + a_{CMP}\Delta h)^2 + b_{CMP}\Delta h^2\ , \tag{18}$$

upon the introduction of the parameters

$$a_{CMP} = p_S + p_G\ , \quad b_{CMP} = t_0\left(\frac{\cos^2\beta_G}{v_G}K^G_{CMP} - \frac{\cos^2\beta_S}{v_S}K^S_{CMP}\right)\ . \tag{19}$$

Unlike Eq. (14), Eq. (18) is no longer a standard NMO-equation but represents a Taylor-expansion around the arbitrary half-offset h_0 chosen for the central ray. The constant-offset case can be easily derived from Eq. (6) and Eq. (11) by setting $\Delta h = 0$. Using the parameter b_{CMP} from the rightmost Eq. (19), we find

$$t^2(m,h_0) = [t_0 + (p_G - p_S)\,\Delta m]^2 + b_{CMP}\Delta m^2. \tag{20}$$

Upon the introduction of the new parameter

$$a_{CO} = p_G - p_S\ , \tag{21}$$

Eq. (20) can be alternatively recast as

$$t^2(m,h_0) = (t_0 + a_{CO}\Delta m)^2 + b_{CMP}\Delta m^2\ , \tag{22}$$

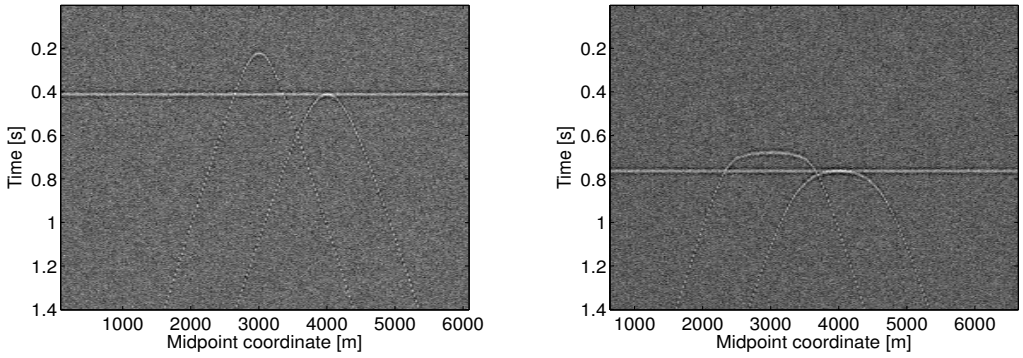

Figure 1: Common-offset sections used for diffraction separation corresponding to a half-offset of 100 m (a) and 650 m (b).

which, in turn, can be regarded as a generalization of Eq. (15) when the central ray has an arbitrary half-offset h_0. Eq. (22) can now be used to enhance diffractions employing the two-step procedure: (i) determine parameters a_{CMP}, b_{CMP} from Eq. (18) and parameter a_{CO} from Eq. (22) using a coherency analysis and (ii) stack data according to Eq. (22) choosing a proper aperture.

Note that the input to this latter stack can be either the constant-offset data or mini-stacked constant-offset data (e.g. the data are stacked within a small offset-range around the chosen half-offset using Eq. (18)).

SYNTHETIC DATA EXAMPLE

Synthetic data were generated for a simple model consisting of a horizontal reflector placed at a depth of 600 m and two point diffractors placed at a depth of respectively 200 m and 600 m. The velocity was set to 2000 m/s. A total number of 240 shot gathers were computed employing a source interval of 25 m. Each shot record consisted of 96 receivers with a group spacing of 25 m. In the simluations a Ricker wavelet with a center frequency of 30 Hz was employed. The data were superimposed white Gaussian noise with a variance of 10% of the maximum (noise-free) trace amplitude.

Diffraction separation in the common-offset domain was tested employing both (i) a ZO central ray and (ii) a constant-offset central ray. Two different half-offsets were considered: 100 m and 650 m. Figures 1(a) and 1(b) show the corresponding common-offset sections.

Zero-offset central ray diffraction separation

Diffraction separation was now carried out based on Eq. (15). Since in this case the NMO-velocity was known use of Eq. (14) was not needed here. However, this NMO-velocity only provide the value of b_{CO} at the apex of the diffractions. In order to obtain the parameter b_{CO} for the complete diffraction traveltime, it is necessary to perform a constrained search within a small range around $\frac{4}{v_{NMO}^2}$. Figures 2(a) and 2(b) show the coherency map for the search of parameters a_{CO} and b_{CO} using semblance (small and large offset respectively). The correspondng diffraction-only sections obtained after a coherency thresholding of 0.2 are shown in Figs 2(c) and 2(d). It can be easily seen from Figs 2(b) and 2(d) that the diffraction separation does not work well in case of a large offset.

Constant-offset central ray diffraction separation

This time the diffraction separation procedure is based on Eqs (18) and (22). First data are sorted in CMP-gathers and a 2-D parameter search is carried out to determine the parameters a_{CMP} and b_{CMP}. Note that this is not a standard NMO-velocity analysis, but a shifted moveout analysis around the (reference) constant-offset trace. Next, for each common-offset section, we use Eq. (22) to determine the parameter

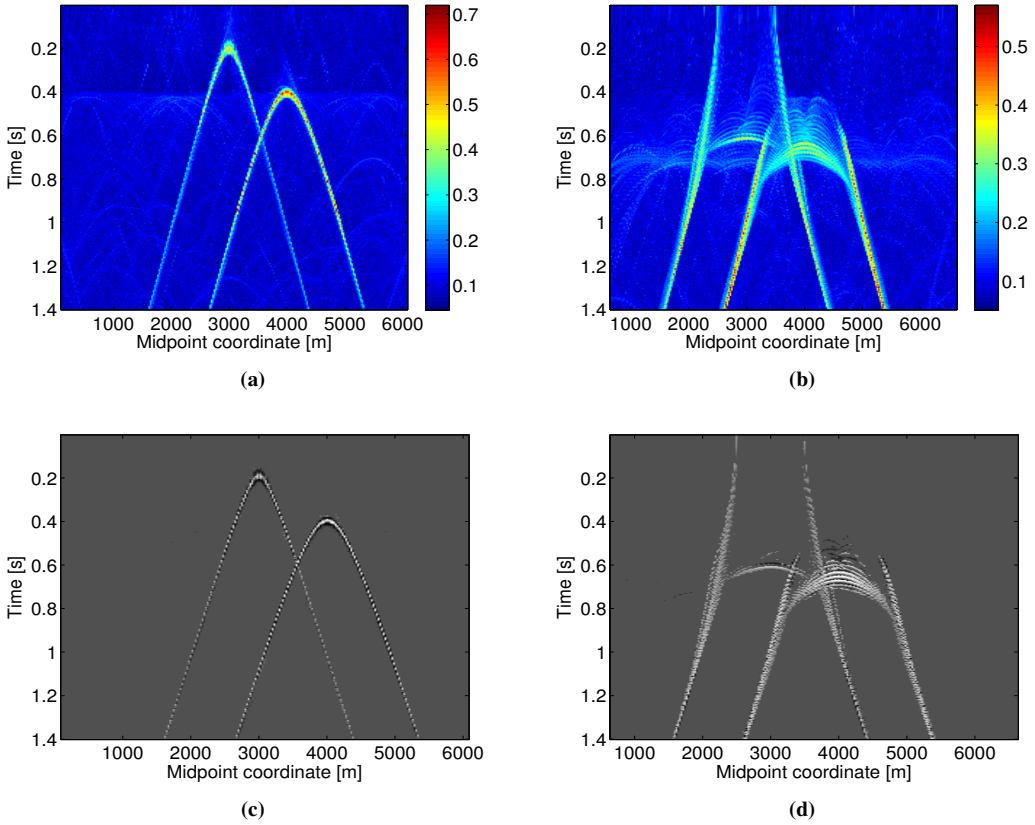

Figure 2: Coherency map based on semblance for small (a) and large (b) offsets. Diffraction only stacked sections for small (c) and large (d) offsets after applying a coherency threshold of 0.2.

a_{CO}. In order to take into account possible inaccuracies we also allow parameter b_{CMP} to vary $\pm 20\%$ around its original value. Thus, in practice also a 2-D parametric search is carried out again but with a constrained b_{CMP}. Figs 3(a) and 3(b) show the coherency map for this 2-D parameter search for the small and large offset respectively.

In order to suppress the reflected energy one needs to use an aperture with a size larger than the first Fresnel zone. However, the CRS traveltime equation in Eq. (22) only works for small apertures. As a consequence, we face a tradeoff between the amount of suppression in the reflected energy and the applicability of the CRS traveltime equation. After selecting an optimal aperture the corresponding diffraction-only stacks are as shown in Figs 3(c) and 3(d). Unlike before, diffraction separation now works also quite well in case of a large offset.

Possible improvements in S/N can be obtained if after the first step in the CMP-domain a mini-stack is performed over a small range of offsets based on the optimal parameter set a_{CMP} and b_{CMP}. The corresponding coherency map for the determination of a_{CMP} and b_{CMP} in a CMP gather for the half-offset of 650 m is shown in Fig 4(a). The corresponding common offset section after mini-stacking in the CMP-domain is shown in Fig 4(b). This section should be compared with the original one in Fig 1(b). The improvement in S/N is clearly demonstrated. The second step of the diffraction separation procedure is carried out in the common-offset domain as described above. The difference here is that the input data is now the common- offset section in Fig. 4(b) and not the original section as given in Fig 1(b). We also used the coherency map in Fig. 4(a) in order to threshold the noise from the signal. The coherency map in Fig. 3(b) is now replaced. Correspondingly, the diffraction-only stack in Fig. 3(d) is replaced by that in Fig. 4(d). Direct comparison between Figs 4(d) and 3(d) shows a slight improvement due to the mini-stacking and the coherency thresholding.

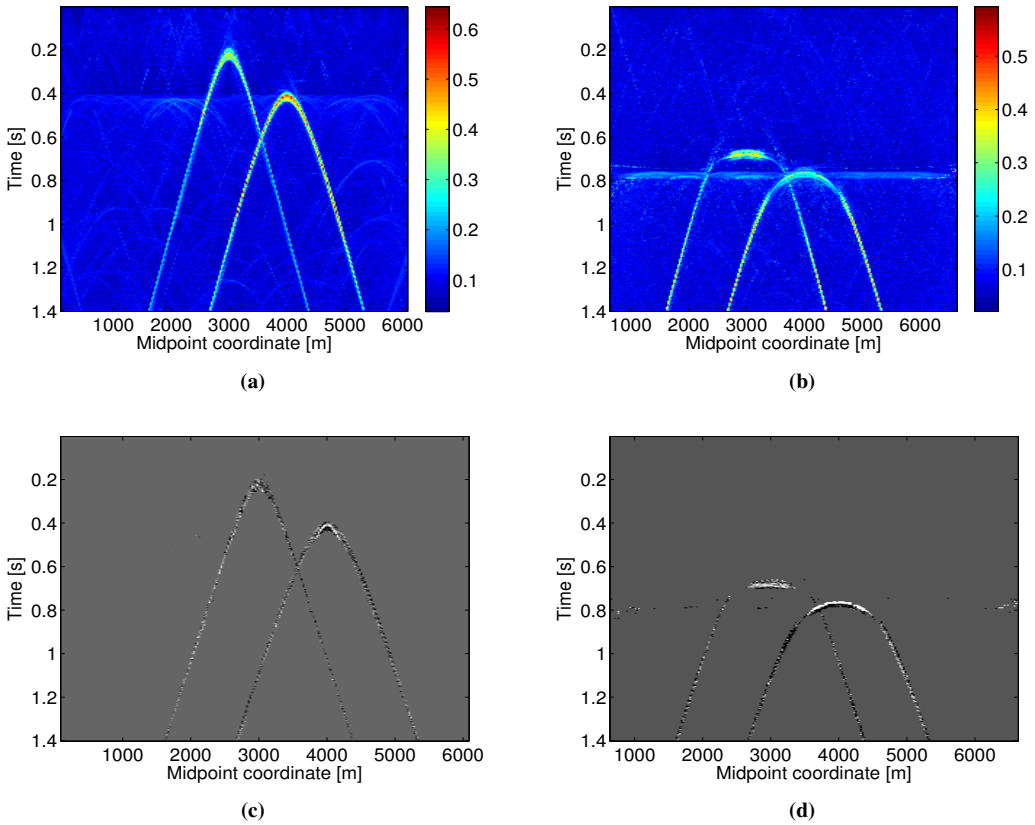

Figure 3: Coherency map based on semblance for small (a) and large (b) offsets. Diffraction only stacked sections for small (c) and large (d) offsets after applying a coherency threshold of 0.2.

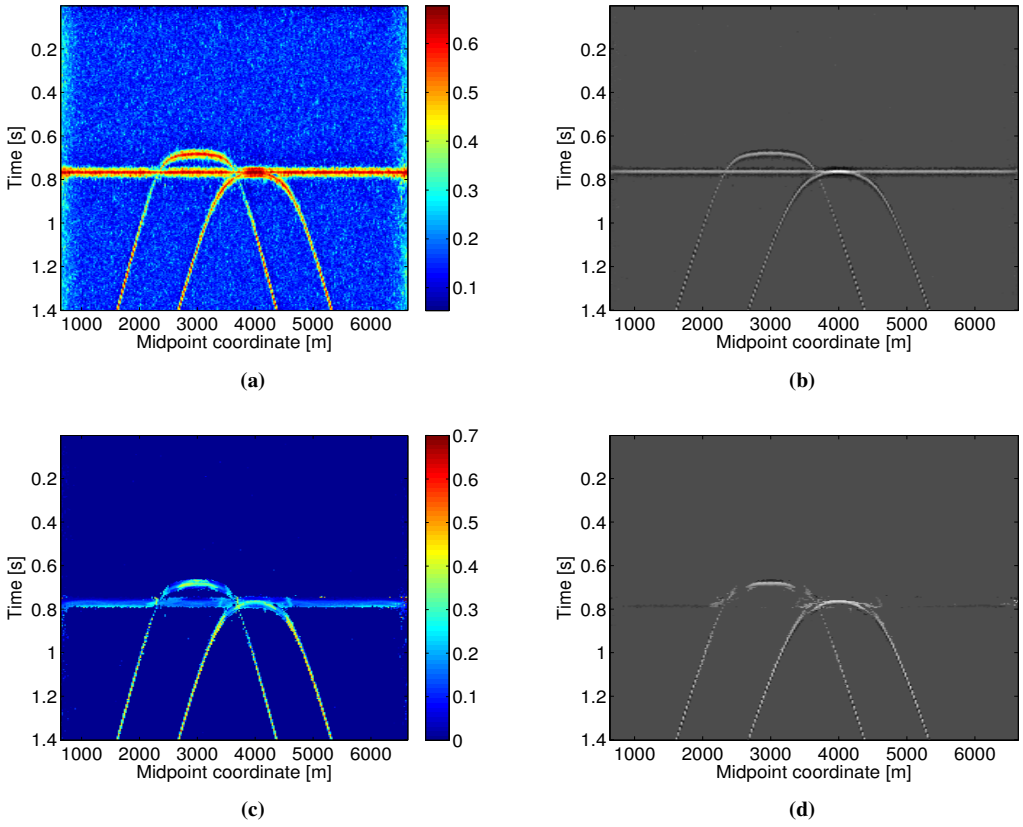

Figure 4: Coherency map based on semblance for the determination of parameters a_{CMP} and b_{CMP} (a). Common-offset section after mini-stack in the CMP domain (b). Coherency map based on semblance for the determination of parameters a_{CO} and b_{CMP} (c). Diffraction only common-offset section after applying a coherency threshold of 0.2 (d).

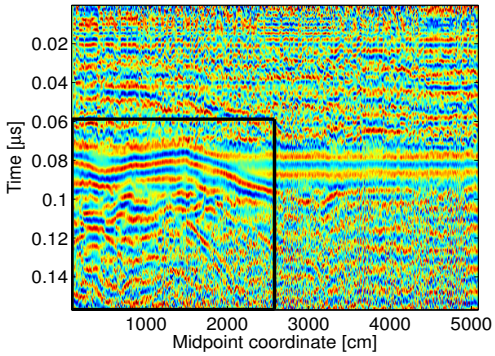

Figure 5: Common-offset section corresponding to a half-offset of 2.5 m used for diffraction separation. The black rectangle indicates the part of the data used for analysis.

GPR DATA EXAMPLE

The Ground Penetrating Radar (GPR) field data is composed of 28 different half-offsets running every 0.1 m from 0.3 to 3 m. The CMP spacing is $0.1m$ covering a $55m$-long profile. Figure 5 shows the common-offset section corresponding to a half-offset of 2.5 m. We can see that almost all the diffracted energy are hidden behind the stronger reflections. Now, following the same procedure as for the synthetic case, we selected part of the data that fall within the black rectangle in Figure 5 and diffractions were separated from reflections employing both ZO and CO central rays. Here, we performed 2-D search directly on CO gathers to obtain parameters a_{CO} and b_{CO} without going to the CMP gathers. The corresponding coherency maps for the ZO and CO central rays respectively are shown in Figs 6(a) and 6(b). It is clear that the CO central ray managed to separate the diffractions for this large offset while the ZO central ray approah did a much poorer job. The diffractions only common-offset section for both approaches are shown in Figs 6(c) and 6(d). Direct comparison shows that the constant-offset ray approach gave a much richer distribution of diffractions.

CONCLUSIONS

A diffraction separation technique that works directly in the common-offset domain has been proposed. It is based on a modified CRS-equation tailored for diffractions. By introducing a constant-offset reference ray, large offsets can also be handled. The feasibility of the method has been demonstrated employing both synthetic and GPR field data.

ACKNOWLEDGMENTS

E. G. Asgedom was funded by the University of Oslo, Department of Informatics. M. Tygel acknowledges support from the National Council of Scientific and Technological Development (CNPq-Brazil). We thank the support of the sponsors of the *Wave Inversion Technology (WIT) Consortium*.

REFERENCES

Asgedom, E. G., Gelius, L. J., and Tygel, M. (2011). A new approach to post-stack diffraction separation. *Extended Abstract. 81st SEG meeting, San Antonio, Texas, USA*.

Fomel, S. (2002). Applications of plane-wave destruction filters. *Geophysics*, 67:1946–1960.

Fomel, S., Landa, E., and Taner, M. (2007). Poststack velocity analysis by separation and imaging of seismic diffractions. *Geophysics*, 72:89–94.

Landa, E., Shtivelman, V., and Gelchinsky, B. (1987). A method for detection of diffracted waves on common-offset sections. *Geophysical Prospecting*, 35:359–373.

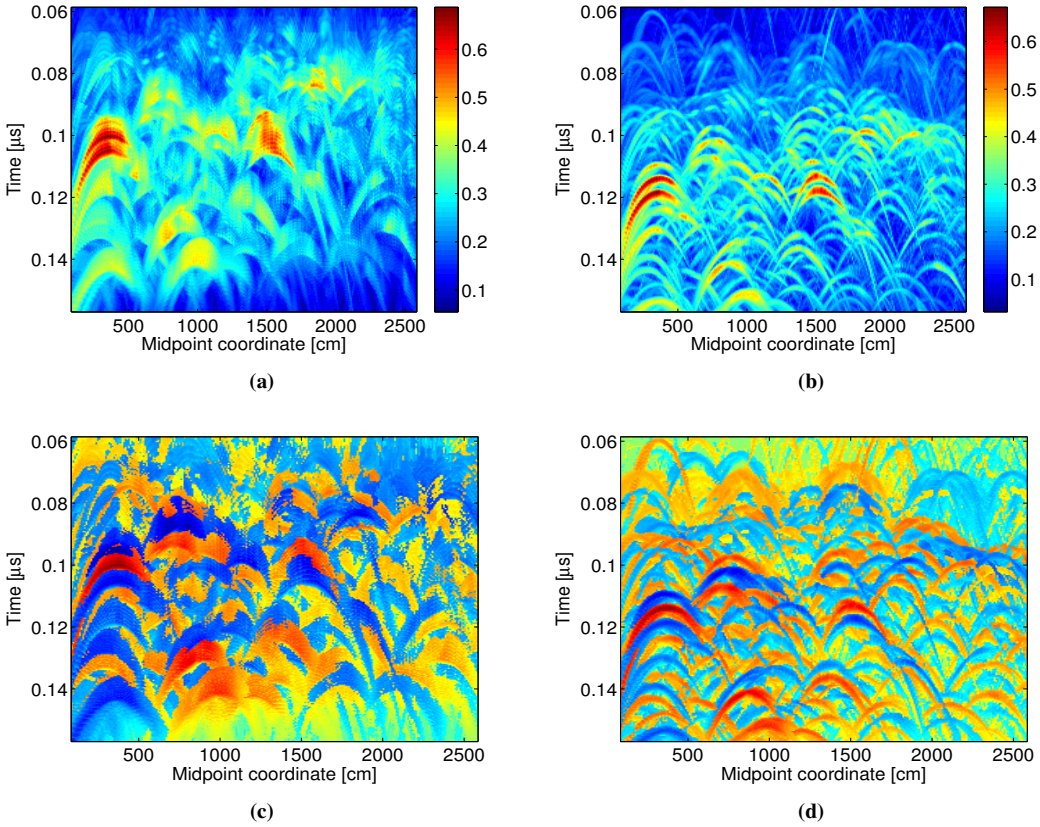

Figure 6: Coherency map based on semblance for the determination of parameters a_{CO} and b_{CMP} based on ZO (a) and CO (b) central rays. Diffraction only common-offset sections after applying a coherency tresholding of 0.1 for ZO (c) and CO (d) central rays.

Ursin, B. (1982). Quadratic wavefront and traveltime approximations in inhomogeneous layered media with curved interfaces. *Geophysics*, 47(7):1012–1021.

Zhang, Y., S., B., and P., H. (2001). Common-reflection-surface (CRS) stack for common offset. *Geophys. Prosp.*, 61(3):759–775.